Quantum Electronics **50** (10) 967–975 (2020)

LASER APPLICATIONS AND OTHER TOPICS IN QUANTUM ELECTRONICS https://doi.org/10.1070/QEL17350

Imaging broadband soft X-ray transmission-grating spectrograph for a wavelength range $\lambda > 111$ Å

A.O. Kolesnikov, E.A. Vishnyakov, E.N. Ragozin, A.N. Shatokhin

Abstract. **A family of aperiodic Mo/Be multilayer mirrors was designed for maximum uniform reflectivity in the ranges 111 – 138, 111 – 150, 111 – 200 and 111 – 222 Å at normal radiation incidence. The simulations took into account the existence of Mo-on-Be and Be-on-Mo transition layers. It was shown that the reflectivity may be as high as 10 % in an octave wavelength range of 111 – 222 Å. We demonstrate the operation of an imaging transmission-grating spectrograph with a broadband Mo/Be multilayer mirror with a uniform reflectivity in the wavelength range 111 – 138 Å synthesised at the Institute for the Physics of Microstructures, RAS. The spectrograph was used to record the line spectra of multiply charged fluorine and magnesium ions from a laser-produced plasma. The role of the grating support structure in the formation of spectral source images is discussed. The spatial resolution of 50 μm is demonstrated.**

Keywords: *soft X-rays, normal incidence, broadband X-ray mirror, aperiodic Mo/Be multilayer structure, laser-produced plasma, transmission diffraction grating, stigmatic spectrograph.*

1. Introduction

In the investigation of laboratory and astrophysical radiation sources in the soft X-ray (SXR) spectral domain it is often necessary to obtain both spectral and spatial information about the source. Instruments that make it possible to obtain a spatially resolved spectrum are imaging spectrographs. One possible version of the optical configuration of such an instrument for the SXR spectral domain is the combination of a concave mirror and a transmission diffraction grating.

Concave mirrors may be employed both in normal-incidence and grazing-incidence configurations. In the latter case, the acceptance angle is small and the spherical mirror possesses irremovable astigmatism, its replacement with a toroidal mirror requiring a significant limitation of the mirror aperture to maintain acceptable image quality [1, 2], which has an adverse effect on the spectrograph luminosity. The Kirkpatrick – Baez configuration [3], which is sometimes used for X-ray imaging, is also characterised by a low luminosity. To obtain high-resolution imaging in grazing-incidence configurations of sufficiently high luminosity, use should be made of more complex optics. For instance, to obtain arc-second angular resolution in the grazing-incidence configuration aboard the AXAF space observatory, advantage was taken of a Wolter type-I telescope, and a system of nested mirrors was employed to improve the telescope luminosity [4].

In the visible and UV regions, a concave spherical mirror mounted at near-normal incidence provides a good image quality for a relatively high luminosity and large angular aperture, since aberrations (with the exception of a low astigmatism) are negligible, provided the aperture is limited to the so-called optimal aperture, which significantly exceeds the angular aperture of a focusing spherical mirror at grazing incidence. And in the Rowland mount of this mirror there is no meridional coma, so that the optimal aperture is limited only by spherical aberration. Unfortunately, the SXR reflection coefficients of the majority of materials are low at normal incidence, and so normal-incidence mirrors have to be coated with multilayer structures, which define the reflectivity spectrum of the mirror and therefore the operating range of the spectrograph as a whole.

The mirrors based on periodic multilayer mirrors possess a resonance reflectivity profile with a high peak reflection coefficient. The spectrograph luminosity can be maximised with the use of a focusing mirror, whose structure period varies across the surface. To this end, the mirror should be placed after the diffraction grating in such a way that the structure period corresponds to the peak reflectivity at the radiation wavelength that arrives from the grating to the corresponding point of the mirror surface. In this case, the grating will operate in a diverging beam. This configuration was realised in Ref. [1]. If the entrance slit is removed and a detector is placed at the mirror focus, the instrument may be employed as an imaging spectroheliograph.

For spectroscopy problems, as a rule, it is necessary that the reflection coefficient remains constant throughout a reasonably broad wavelength range. This reflectivity spectrum is inherent in aperiodic multilayer structures, which were proposed for X-ray astronomy in 1987 [5], each layer thickness being considered as an independent optimisation parameter. This approach, which involves optimisation of multilayer structures, turned out to be suited to the solution of a variety of problems. It was used, for instance, to calculate structures with the maximum integral reflection coefficient or with maximum uniform reflectivity at a fixed wavelength in a specified range of incidence angles or at a fixed incidence angle in a specified wavelength range [6, 7].

A.O. Kolesnikov Lebedev Physical Institute, Russian Academy of Sciences, Leninsky prosp. 53, 119991 Moscow, Russia; Moscow Institute of Physics and Technology (National Research University), Institutskii per. 9, 141701 Dolgoprudnyi, Moscow region, Russia; e-mail: alexey6180@gmail.com;
E.A. Vishnyakov, E.N. Ragozin, A.N. Shatokhin Lebedev Physical Institute, Russian Academy of Sciences, Leninsky prosp. 53, 119991 Moscow, Russia

Received 14 April 2020; revision received 28 May 2020
Kvantovaya Elektronika **50** (10) 967–975 (2020)
Translated by E.N. Ragozin

By 2000, an algorithm was developed at the Lebedev Physical Institute (LPI), which was intended for the numerical solution of different problems of multilayer structure optimisation [8, 9]. Following the simulations made at the LPI, broadband mirrors based on an aperiodic Mo/Si structure optimised for maximum uniform reflectivity in the 125–250 Å wavelength range were synthesised at the Kharkov Polytechnic Institute in 2001 [10]. The simulations included 6-Å thick Si-on-Mo and 12-Å thick Mo-on-Si transition layers with a stoichiometry of $MoSi_2$. The mirrors possessed a uniform reflectivity at a level of 14% and since then were repeatedly used in experiments to record stigmatic plasma spectra [12], the spectra of a laser-produced plasma in a pulsed xenon jet [13, 14], in the investigation of the charge exchange of multiply charged ions with the atoms of an inert gas [15, 16], in the reflection of laser radiation from the relativistic wave of electron density in a laser-produced plasma (the relativistic 'flying mirror') [17], as well as in the harmonic generation at the singularities of plasma electron density in the multiflow motion driven by multiterawatt femtosecond laser irradiation [18]. Recently, a broadband high-resolution imaging spectrograph was implemented at the LPI, which was based on a reflection plane VLS grating and the broadband Mo/Si mirror serving as a focusing element [19, 20].

Since Mo/Si structures are efficient at wavelengths $\lambda >$ 125 Å due to the silicon L absorption edge in the vicinity of 125 Å, advancement to the shorter-wavelength domain calls for the use of other elements instead of silicon. Estimative simulations suggested that beryllium is the element of choice: the expected uniform reflectivity of a Mo/Be structure may be about 20% throughout the range 111–135 Å [21]. In 2014, in connection with the launch of the laboratory for the synthesis of beryllium-containing mirrors at the Institute for the Physics of Microstructures (IPM) of the Russian Academy of Sciences in Nizhny Novgorod, there emerged a possibility of synthesising these structures in our country. To date, the IPM RAS has accumulated considerable experience in the synthesis of periodic beryllium-containing multilayer structures, and developed methods for reconstructing the structure parameters from hard and soft X-ray reflectometry [22, 23], electron microscopy [24], and mass spectrometry [25].

In the optimisation of multilayer structures, the densities of layered materials are set constant. However, the material density depends, generally speaking, on the layer thickness: As shown in Ref. [26], the density of molybdenum varies from 75% to 97% of the tabular value under variation of the layer thickness from 15 to 55 Å. Monitored in the course of synthesis is the deposition time of a material and therefore its amount rather than the layer thickness. That is why the layer thicknesses of a synthesised aperiodic structure may significantly differ from the design thicknesses, which will affect its reflectivity spectrum. To avoid this, Kozhevnikov et al. [27] came up with the idea to modify the merit function in such a way as to decrease the thickness variations of the neighbouring layers of the same material. By the example of the Mo/Si mirror optimisation for uniform reflectivity at a wavelength of 135 Å in a broad angular range, they showed that it is possible to significantly reduce the spread of layer thicknesses at the expense of an insignificant lowering of the reflectivity and its slightly higher angular nonuniformity.

There is an alternative approach to the production of broadband SXR multilayer mirrors proposed by Kuhlman, Yulin, et al [28]: the design of stack structures, which involves the sequential deposition of several different periodic structures on top of each other. Owing to the smaller number of parameters, these structures are easier to control in the course of synthesis, what makes them technologically preferable. However, the limiting possible reflection coefficient and its spectral uniformity for stack structures turn out to be lower than for completely aperiodic ones, since the stack structures are a subset in the set of aperiodic structures. Broadband mirrors for the spectral range 111–138 Å made up of a stack Mo/Be structure were synthesised at the IPM RAS on spherical (radius, 1 m) substrates of fused silica made at the LPI [29].

The aim of our work was to consider the possibility of designing aperiodic Mo/Be multilayer structures optimised for maximum uniform reflectivity in a broad (up to an octave) wavelength range, to calculate these structures with the minimisation of the spread of layer thicknesses, as well as to demonstrate the operation of an imaging diffraction spectrograph with a transmission grating and a broadband mirror with a Mo/Be stack structure synthesised at the IPM RAS and obtain line spectra from a laser-produced plasma in the 111–138 Å range with spatial resolution.

2. Optimisation of Mo/Be aperiodic multilayer structures

Classically, the problem of optimising an aperiodic multilayer structure for maximum uniform reflectivity in the wavelength range from $\lambda_{\min}$ to $\lambda_{\max}$ is reduced to minimising the meri function of the form

$$F = \int_{\lambda_{\min}}^{\lambda_{\max}} [R(\lambda, \boldsymbol{d}) - R_0]^{2m} \mathrm{d}\lambda, \qquad (1)$$

where $R(\lambda, \boldsymbol{d})$ is the reflection coefficient of the structure at a wavelength λ; $\boldsymbol{d}$ is the vector of structure layer thicknesses; m is a positive integer; and R_0 is the goal value of the reflection coefficient. The minimisation is performed numerically, for instance, by the method of steepest descent or with the use of a genetic algorithm. The resultant structure possesses, as a rule, a significant spread of layer thicknesses, which is inconvenient for its synthesis. The spread of thicknesses may be considerably decreased by modifying the merit function in the following way:

$$F = \int_{\lambda_{\min}}^{\lambda_{\max}} [R(\lambda, \boldsymbol{d}) - R_0]^{2m} \mathrm{d}\lambda + c \sum_{i=\Delta n+1}^{N} (d_i - d_{i-\Delta n})^{2m}, \qquad (2)$$

where c is the smoothing coefficient; Δn is the 'smoothing period' (the difference of closest layer numbers whose thicknesses should be brought closer to each other); N in the number of layers in the structure; and d_i is the ith layer thickness. For $\Delta n = 2$, the thicknesses of the nearest layers of the same material will be brought closer, like in Ref. [27], while brought closer for $\Delta n = 1$ are the thicknesses of all neighbouring layers. In the latter case, the dependence of the layer thickness on the layer number will look like a smooth curve.

To calculate broadband Mo/Be mirrors, we modified the programme developed in Refs [8, 9] so as to make the resultant structures more suitable from the standpoint of their synthesis as well as to investigate the effect of smoothing parameters c and Δn on the reflectivity spectrum of the structures. The optimisation was performed by the method of steepest descent, a periodic structure was taken as the initial one, $m = 1$, $\lambda_{\min} = 111$ Å, and $N = 82$ in all simulations. Account was

taken of Mo-on-Be (σ = 7 Å) and Be-on-Mo (σ = 3 Å) transition layers [24], where σ is half the thickness of the transition layer. The angle of radiation incidence on the mirror is 5°. The upper layer of the structure is Be, and the substrate of fused silica SiO_2 has a root-mean-square surface roughness of 3 Å. Other factors that lower the light intensity in the specular direction are the interlayer roughness and the interdiffusion of materials at the layer boundaries. They are taken into account using a unified characteristic: the thickness of a transition layer. In our simulations we used the optical constants data for Mo and Be published in Refs [30, 31] and posted on the site of the Lawrence Berkeley National Laboratory [32].

According to investigations involving the reconstruction of Mo/Be structures performed at the IPM RAS, the upper beryllium layer is partly oxidised to form an uppermost 14-Å thick layer of BeO [29]. Comparing the reflection coefficients of the simulated structure (with neglect of the oxidation) and the synthesised structure with the formation of the oxide layer showed that the partial oxidation of the upper Be layer had only a slight effect on the structure reflectivity. This comparison was made for the stack Mo/Be structures optimised for maximum uniform reflectivity in the range 111–138 Å [29]. That is why the oxide formation was neglected in the simulations.

3. Analysis of the simulation data for Mo/Be mirrors

In quest of the possibilities of making broadband mirrors based on aperiodic Mo/Be structures, we performed a series of simulations of the structures optimised for uniform reflectivity in four spectral ranges: 111–138 Å, 111–150 Å, 111–200 Å, and 111–222 Å. Figure 1 depicts the calculated reflectivity spectra of these structures. With broadening the spectral range, the reflectivity plateau height becomes lower to reach a level of 10% for an octave-wide range. The average reflection coefficient R of the first, second, third, and fourth structure is 15.8%, 12.6%, 10.7%, and 10.3%. The fourth structure is also capable of reflecting at longer wavelengths: its reflection coefficient decreases smoothly (almost linearly) from 10% at λ = 220 Å to 5% at λ = 290 Å. The integral reflectivity of the structures increases with broadening the optimisation range. The relative rout-mean-square reflectivity deviation R from the structure plateau level is 3.2%, 5.5%, 7.6%, and 5.8%, respectively.

To analyse the effect of the smoothing coefficient on the reflectivity spectrum of a broadband Mo/Be multilayer mirror, we performed a series of simulations and, in doing this, for the upper bound of the optimisation range we adopted λ_{max} = 138 Å. In doing this, we employed the same initial periodic structure, the smoothing period was Δn = 2, and the smoothing coefficient c was varied from zero to increasing positive values. The dependences of the resultant structure characteristics on the smoothing coefficient c are plotted in Fig. 2. As one can see, with increasing c, the plateau level hardly changed and became slightly lower than 16%. In this case, the root-mean-square nonuniformity σ_R of the spectral reflection coefficient increases monotonically (and with deceleration). For small c, the spread of layer thicknesses d_{max}/d_{min} varies rapidly, but even for $c \approx 2 \times 10^{-4}$ Å^{-1} it is hardly changes. The further growth of the smoothing coefficient does not change the maximal spread of layer thicknesses but makes smoother the dependence of the layer thickness on its

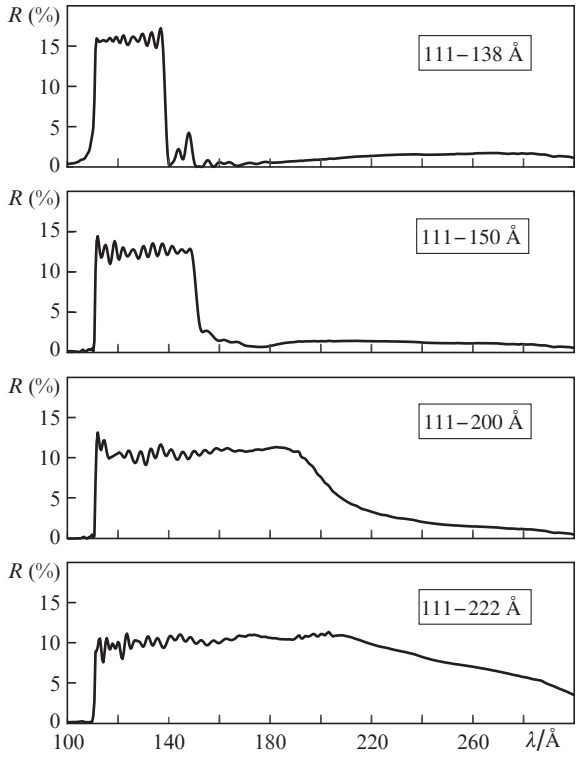

Figure 1. Reflectivity spectra of the aperiodic Mo/Be structures optimised for maximum uniform reflectivity in different ranges.

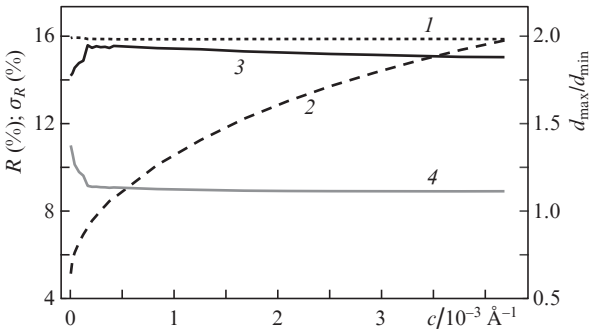

Figure 2. Effect of smoothing on the result of aperiodic Mo/Be multilayer structure optimisation for maximal uniform reflectivity in the range 111–138 Å; (*1*) absolute reflection coefficient R averaged over the spectral range; (*2*) relative root-mean-square deviation σ_R of the reflection coefficient; (*3*) and (*4*) maximum-to-minimum layer thickness ratio d_{max}/d_{min} in the structure for beryllium and molybdenum, respectively.

number, the uniformity of the spectral reflectivity deteriorating in this case.

The optimal smoothing coefficient corresponds to the situation when both the spread of molybdenum layer thicknesses is small (ceases to vary) and the nonuniformity of the reflection coefficient is minimal, and therefore the optimal c value is about 2×10^{-4} Å^{-1}. Attainable for this value are a good uniformity of the reflectivity and the minimal departure of the deposited Mo layer thicknesses from the design ones, since the density of Mo may be assumed to be the same for all layers with a good accuracy. We note that obtaining a

smoother dependence of the layer thickness on the layer number may be useful in terms of ease of synthesis. In the synthesis of aperiodic structures, the facility must first be calibrated in terms of all layer thickness; consequently, the number of calibrations is generally equal to the number of layers in the structure (about a hundred by the order of magnitude) [29]. However, when all layers vary little in thickness (apart from maybe a few ones), the number of preliminary calibrations may be considerably reduced. It would be sufficient to perform about five calibrations in the range of thickness variation of the majority of layers and one calibration per each layer that is strongly different from the others (for large c, no more than one layer for each material). In the synthesis of such a structure, it would be quite correct to take advantage of interpolation between the calibration points.

Figure 3 depicts the reflection spectra and the dependences of layer thicknesses on the bilayer number for the four Mo/Be structures optimised for maximum uniform reflectivity in the 111–138 Å range for different c and Δn. One can see how the smoothing coefficient c affects the spectrum and the structure. Initially, the spectrum hardly changes, and in Fig. 3d the peaks sink and the dips become shallower. As c is increased further, the spectral uniformity deteriorates, but the number and amplitudes of the peaks and dips decrease: the dependence of layer thickness on the number becomes smoother. An extraordinary feature of all structures optimised for the 111–138 Å wavelength range is the increasing dependence of the layer thickness on its number (the number increases from the surface to the substrate).

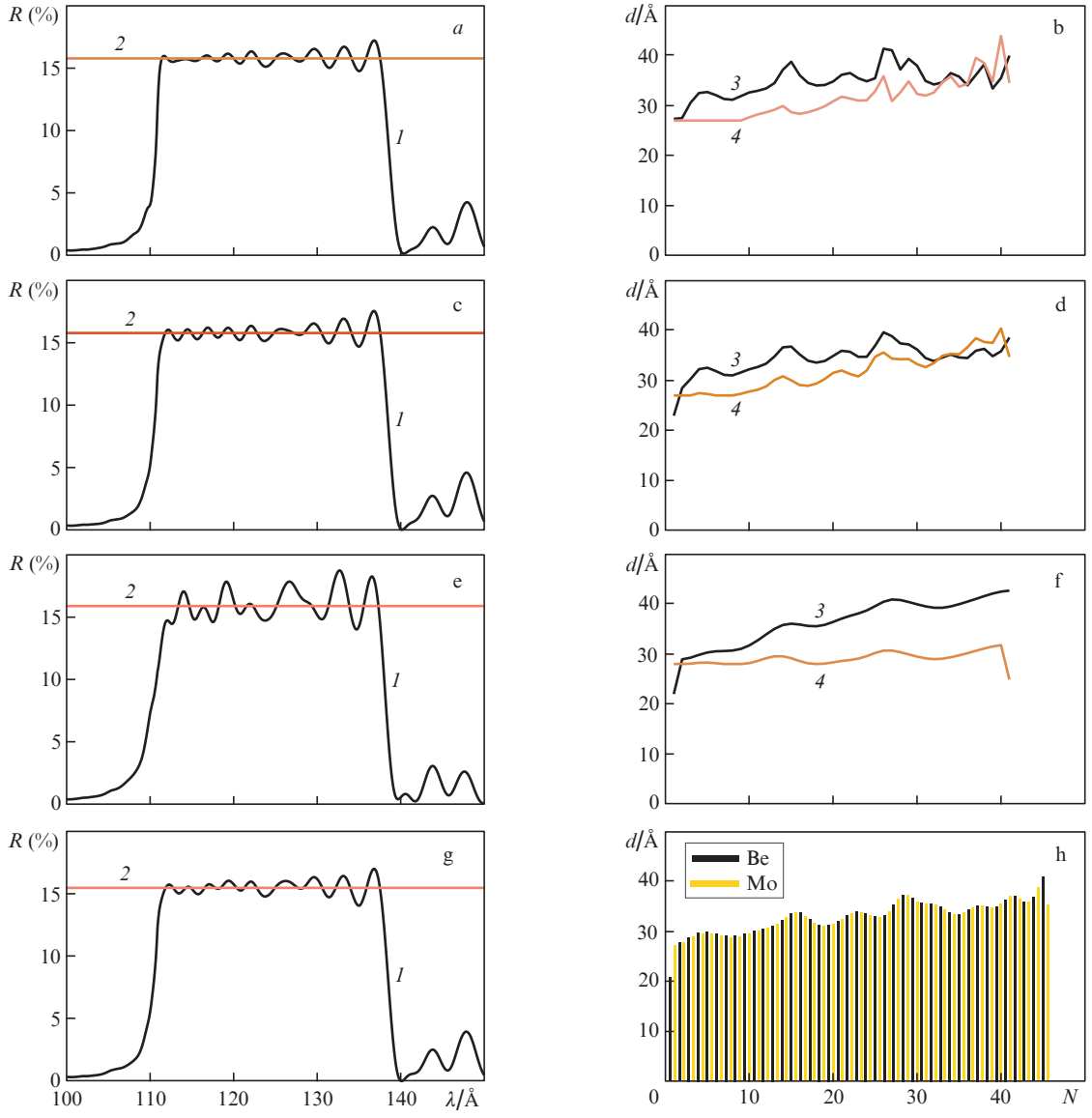

Figure 3. Spectral reflectivities of four Mo/Be structures optimised for maximum uniform reflectivity in wavelength range 111–138 Å (a, c, e, g) and layer thicknesses of these structures (b, d, f, h) for $c = 0$, $c = 9 \times 10^{-5}$ Å^{-1} and $\Delta n = 2$ (c, d), $c = 4.2 \times 10^{-4}$ Å^{-1} and $\Delta n = 2$ (e, f), $c = 2.0 \times 10^{-5}$ Å^{-1} and $\Delta n = 1$ (g, h); (*1*) spectral reflectivity of the structure; (*2*) plateau level; (*3*) beryllium layers; (*4*) molybdenum layers. The bilayer number increases from the surface to the substrate. The number of layers is 82 (41 pair), the upper layer is beryllium, the lower level is molybdenum; N is the bilayer number.

Interestingly, the smoothing for 111–138 Å range for $\Delta n = 1$ may lead to a better simulation result. One can see that the structure (the fourth) with this Δn (Figs 3g and 3h) offers a slightly lower (~15.5%) reflectivity R than the remaining ones (~15.8%) but possesses the same uniformity as the second one ($\sigma_R \approx 4\%$). In this case, the spread of molybdenum layer thicknesses for the fourth structure is smaller (the maximal layer thickness is 39 Å and the minimal one is 27 Å) than for the second structure (the maximal layer thickness is 40.4 Å and the minimal one is 27 Å), and therefore this structure is optimal from the standpoints of spectrum quality and ease of synthesis.

Similar simulations (without smoothing, smoothing for $\Delta n = 2$ and 1) were also performed for the structures with uniform reflectivity in the ranges 111–150 Å and 111–200 Å. In these structures, the layer thicknesses decrease with increasing layer number. For the 111–150 Å range, the R and σ_R values were 12.5% and 5.5% (without smoothing), 12.42% and 6.17% (optimal smoothing for $\Delta n = 2$), and 12.41% and 6.00% (optimal smoothing for $\Delta n = 1$). In this case, the spread of molybdenum layer thicknesses hardly changed: from 20 to 35 Å in the absence of smoothing, as well as for the optimal smoothing for $\Delta n = 2$, and from 20 to 37 Å for the optimal smoothing for $\Delta n = 1$. For the 111–200 Å range, the R and σ_R values were 10.67% and 7.66% (without smoothing), 10.50% and 9.52% (optimal smoothing for $\Delta n = 2$), and 10.54% and 8.46% (optimal smoothing for $\Delta n = 1$). In this case, the molybdenum layer thicknesses range from 20 to 45 Å in the first two cases and from 20 to 49 Å for $\Delta n = 1$. Therefore, with increasing range width, the smoothing for $\Delta n = 1$ ceases to reduce the spread of molybdenum layer thicknesses, and in the case of optimisation in the 111–222 Å range the use of the parameter $\Delta n = 1$ does not permit smoothing the spread of layer thicknesses with retention of the uniformity of spectral reflectivity.

Broadening the wavelength range will be inevitably accompanied by the difference between the maximal and minimal layer thicknesses, which is impossible to decrease by smoothing. In the optimisation of the structure for maximum uniform reflectivity in a wavelength octave, smoothing will lower the reflectivity of the structure, especially so in the long-wavelength part of the spectrum, the nonuniformity of spectral reflectivity being mainly due to this circumstance. Therefore, when the optimisation wavelength range is broad, the efficiency of smoothing is low and the optimal value of the c coefficient is close to zero (Fig. 4). The effect of optimal smoothing on the mirror optimisation result in the 111–222 Å wavelength range is exemplified in Fig. 5. One can see that the smoothing, for the most part, decreases the number of oscillations of layer thickness, making smoother the dependence of the layer thickness on the number of the layer. In this case, the reflectivity spectrum is hardly changed.

Therefore, there is a possibility of making broadband mirrors based on aperiodic Mo/Be multilayer structures in the wavelength region above 111 Å. For a wavelength range narrower than an octave, the smoothing makes it possible to obtain a technologically more convenient structure with hardly any lowering of the reflection coefficient and its uniformity. In broader wavelength ranges, the smoothing turns out to be less efficient and can offer only an insignificant decrease in the number of preliminary calibrations before the synthesis procedure. For an octave-broad range, the attainable uniform reflection coefficient is about 10% for a relative root-mean-square nonuniformity of about 6%.

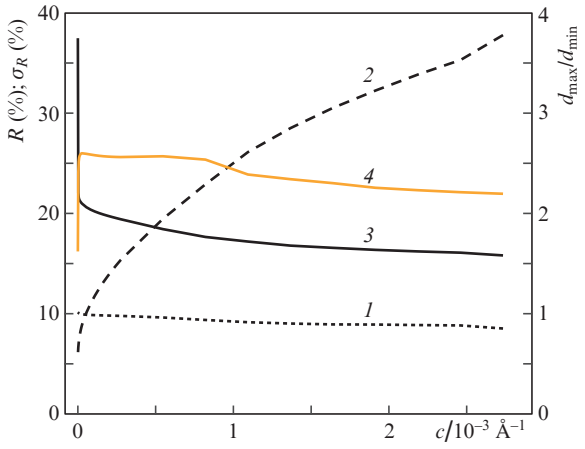

Figure 4. Characteristics of the aperiodic Mo/Be multilayer structure optimised for maximum uniform reflectivity in the 111–222 Å range plotted as functions of the smoothing coefficient c. The notation and the numbers of curves *1–4* are the same as in Fig. 2. The lowering of R and the growth of σ_R occur due to the reflectivity lowering in the long-wavelength part of the working range.

4. Imaging diffraction spectrograph in the wavelength range 111–138 Å

The spectrograph is shown schematically in Fig. 6. This configuration was earlier employed in the range 125–250 Å. For a focusing element, use was made of a broadband mirror based on an aperiodic Mo/Si structure synthesised in the Kharkov Polytechnic Institute [13–16]. The mirror places on the detector the horizontal image of the entrance slit and the vertical image of the source, thereby providing spatial resolution along the entrance slit. In this case, the magnification coefficients are close to unity. The transmission grating operates in the converging beam produced by the mirror. The operating spectral range of the instrument (125–250 Å) was limited by the reflection spectrum of the Mo/Si mirror. To advance to the shorter-wavelength domain, it was decided to make broadband mirrors based on a Mo/Be structure.

The Mo/Be mirrors were synthesised at the IPM RAS. All mirrors were based on the same simulated six-stack multilayer structure. The spherical substrates of radius 1 m were made at the LPI. According to the measurements performed on the reflectometer of the IPM RAS [23], in the wavelength range 111 – 138 Å the mirrors exhibit a reflectivity R of ~14.3% for a relative root-mean-square reflectivity nonuniformity $\sigma_R \approx 9.4\%$ (Fig. 7).

The imaging diffraction spectrograph was assembled and aligned in a cylindrical (diameter, 0.9 m; length, 3.8 m) vacuum chamber equipped with an oil-free pump system (residual pressure, 10^{-5} Torr). The role of the focusing element was fulfilled by the stack Mo/Be mirror. The detector was a CCD array with square 13-μm pixels (Teledyne e2v, Great Britain). The working lines of the transmission grating were vertically oriented and the dispersion plane was horizontal. The line density was 989 mm^{-1} and the duty ratio (the ratio of the opening between the lines and the period) was about 0.44. The grating–detector distance was ~336 mm, the entrance slit was 15 μm wide, and the slit--source distance was ~35 mm. The spectral resolution was defined by the detector pixel size (13 μm) and was numerically equal to the product of the plate

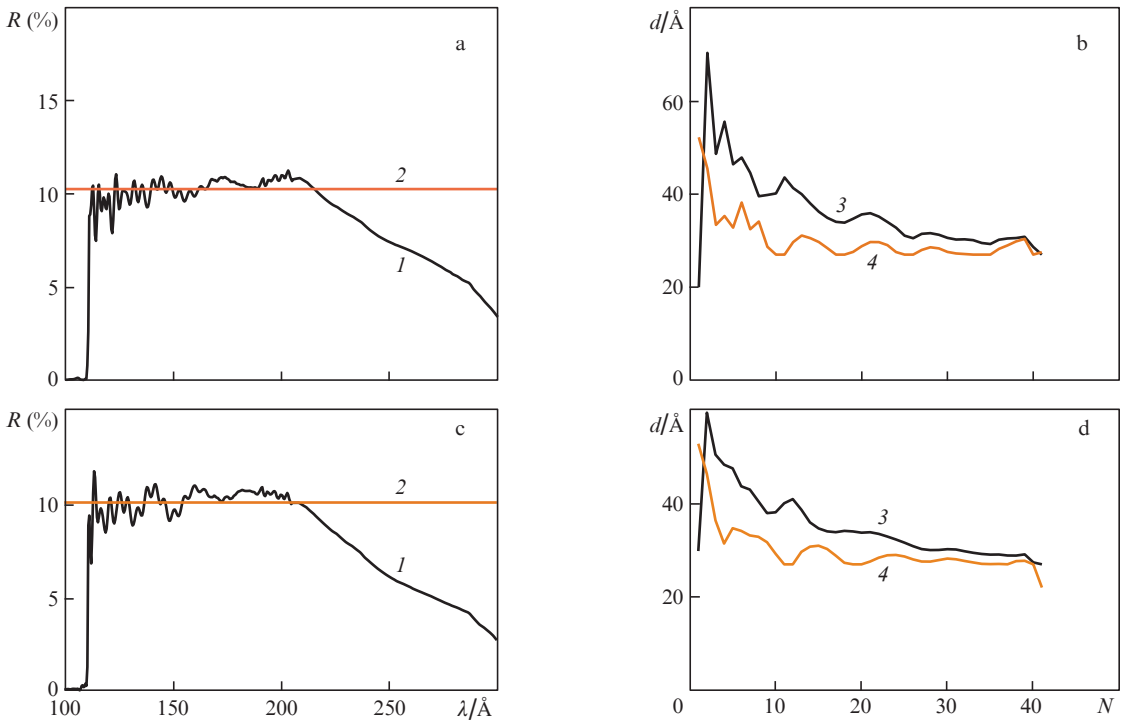

Figure 5. Spectral reflectivity (*1*) and plateau level (*2*) for the Mo/Be structures optimised for maximum uniform reflectivity in the range 111–222 Å (a, c) as well as Be (*3*) and Mo (*4*) layer thicknesses in the optimisation without smoothing (a, b) and with smoothing for $c = 2.7 \times 10^{-6}$ Å^{-1} and $\Delta n = 2$ (c, d); N is the bilayer number.

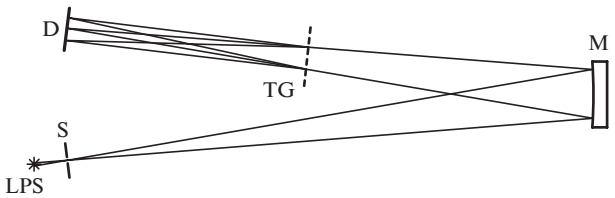

Figure 6. Schematic diagram of the imaging spectrograph with a transmission grating and a broadband multilayer mirror:
(LPS) laser-plasma source; (S) entrance slit; (M) broadband focusing multilayer mirror; (TG) transmission diffraction grating; (D) detector.

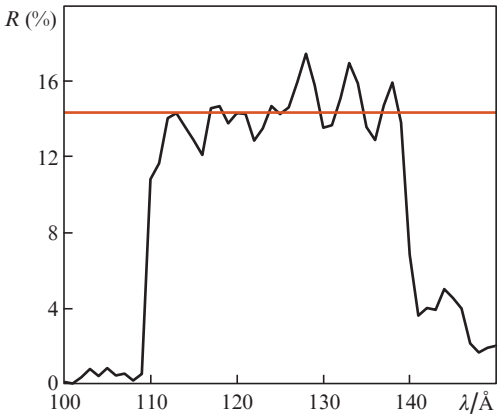

Figure 7. Spectral reflection coefficient of the broadband mirror based on a six-stack Mo/Be structure measured at the IPM RAS. The straight line denotes the reflectivity averaged over the 111–138 Å range.

scale (30.09 Å mm^{-1}) and the doubled pixel size (26 μm), which yields 0.78 Å. In this case, the spectral resolving power at the centre of the operating spectral range is $\lambda/\delta\lambda \approx 160$ at a wavelength of 125 Å.

The grating has a complex regular support structure: a square structure with a spatial frequency less than 1 mm^{-1}, a square one with a frequency of ~5 mm^{-1}, and a horizontal one with a frequency of ~49 mm^{-1} (Fig. 8). The last one has a duty ratio of about 0.55. The spatial frequencies of the grating lines and support structures as well as of their duty ratios were measured from the diffraction of He–Ne laser radiation.

The diffraction from the first two support structures in the operating spectral range is too weak (both in angle and intensity) to be resolved by the detector (the separation of the diffraction orders is less than two detector pixels). The diffraction by the last-named (horizontal) one will result in the overlap of the source images in different diffraction orders, with the effect that the spatial distribution of the source intensity in the vertical direction will not correspond to its image on the detector. That is why reconstructing the spatial profile of a spectral line calls for the solution of the inverse problem.

The observed intensity distribution of a spectral line with height h is described by the formula

$$I_{\text{obs}}(h) = I(h) + \alpha_1[I(h-a) + I(h+a)] + \alpha_2[I(h-2a) + I(h+2a)] + \ldots, \quad (3)$$

where $I(h)$ is the desired intensity distribution (the zeroth order of diffraction from the horizontal support structure);

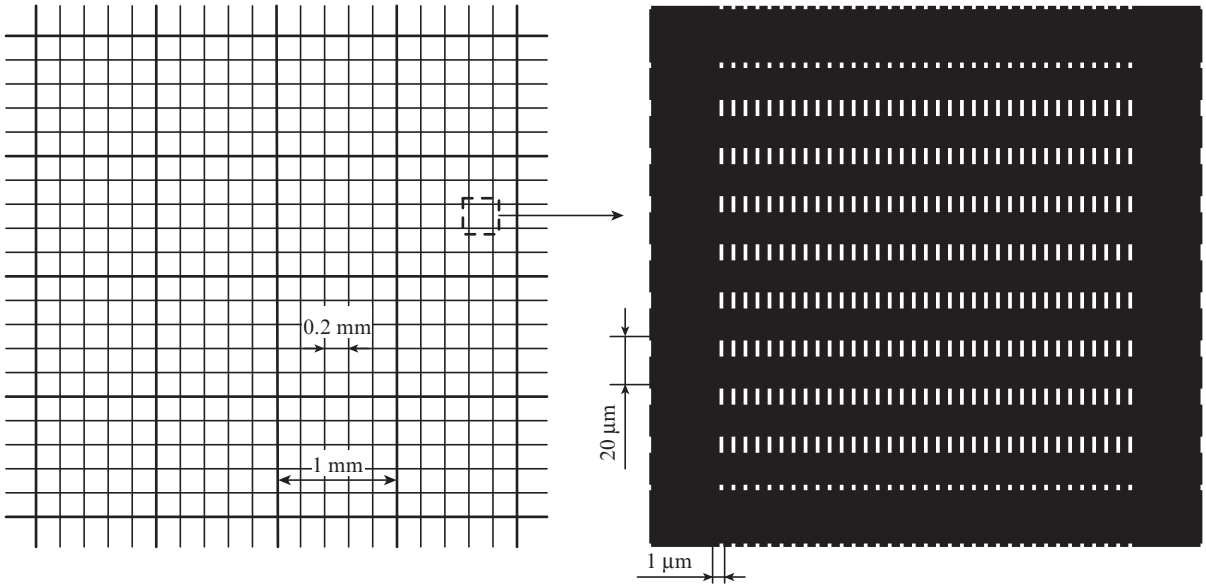

Figure 8. Schematic representation of the free-standing transmission grating and its support structure. At the left: two coarse square support structures with sides of about 1 and 0.2 mm. At the right: an elementary cell of the square structure with a side of ∼0.2 mm; one can see a horizontal fine support structure with a duty ratio of ∼0.55 and a period of ∼20 μm as well as the working grating lines (not to scale) with a period of about 1 μm.

α_i is the relative intensity of the ±ith diffraction order; $a = (\lambda/d_{\text{hs}})/L$ is the shift caused by the structure; d_{hs} is the period of the horizontal support structure; and L is the grating–detector distance. The greatest contribution is made by the first order of diffraction by the support structure, whose intensity amounts to about 30% of the zeroth one, while the contribution from the second and third orders is less than 3%. This signifies that $\alpha_1 \sim 0.3$, while α_2 and $\alpha_3 \sim 0$. Then the signal read from the detector pixel with number k is of the form:

$$I_k = I_k^0 + \alpha_1(I_{k+\Delta k}^0 + I_{k-\Delta k}^0), \tag{4}$$

where I_k^0 is the desired spectral line profile and Δk is the distance between the zeroth and first diffraction orders expressed in terms of the number of detector pixels. This opens up the possibility to reconstruct the profile using the method of gradient descent and consider I_k^0 as independent optimisation parameters. For the merit function, use can be made of the expression

$$F = \sum_k (I_k^{\text{exp}} - I_k)^2 = \sum_k [I_k^{\text{exp}} - I_k^0 - \alpha_1(I_{k+\Delta k}^0 + I_{k-\Delta k}^0)]^2, \tag{5}$$

where I_k^{exp} is the kth pixel reading obtained in experiment. Then, the kth term of the gradient of F is given by the formula

$$\frac{\partial F}{\partial I_k^0} = -2[I_k^{\text{exp}} - I_k^0 - \alpha_1(I_{k+\Delta k}^0 + I_{k-\Delta k}^0)] - 2\alpha_1[I_{k+\Delta k}^{\text{exp}} - I_{k+\Delta k}^0 - \alpha_1(I_{k+2\Delta k}^0 + I_k^0)] - 2\alpha_1[I_{k-\Delta k}^{\text{exp}} - I_{k-\Delta k}^0 - \alpha_1(I_k^0 + I_{k-2\Delta k}^0)] = -2(I_k^{\text{exp}} - I_k) - 2\alpha_1[(I_{k+\Delta k}^{\text{exp}} - I_{k+\Delta k}) + (I_{k-\Delta k}^{\text{exp}} - I_{k-\Delta k})], \tag{6}$$

and the iterative descent procedure takes the form

$$I_k^0(i+1) = I_k^0(i) - \frac{\partial F}{\partial I_k^0}\tau, \tag{7}$$

where τ is the iteration step. The descent was performed several times to find the best values of parameters α_1 and Δk.

To demonstrate the imaging properties of the instrument, we recorded the laser-produced plasma spectra of LiF and Mg targets with spatial resolution. Figure 9 shows the stigmatic spectrum of a lithium fluoride plasma recorded in one Nd:YAG laser shot (0.5 J, 8 ns). One can see the brightest line arrays of the ions Li III and F V–F VII. Also discernible is the crossed diffraction pattern due to the support structure, which involves the zeroth and two first diffraction orders.

In the course of further processing of the spectrum, we recorded the profile of the spatial intensity distribution of the $\lambda = 127.7$ Å line of F VII. The order separation problem for the diffraction from the support structure was solved by the method of gradient descent with the subsequent approximation of the resultant profile by a smooth curve. The result of reconstruction and the experimentally recorded and reconstructed images in the detector plane are plotted in Fig. 10.

Three Nd:YAG laser shots were used to record the stigmatic spectrum of magnesium plasma, which contained a wealth of Mg IV–Mg VI ion lines in the 111–138 Å wavelength range (not given in the paper).

Therefore, the Mo/Be mirror underlay the operation of the imaging diffraction spectrograph in the range 111–138 Å. The demonstrated spectral resolving power of the instrument (about 160) is limited by two detector pixels. The spatial resolution of the instrument may be estimated from the width of the light–shadow boundary: it amounts to about four detector pixels, which corresponds to ∼50 μm (Fig. 10).

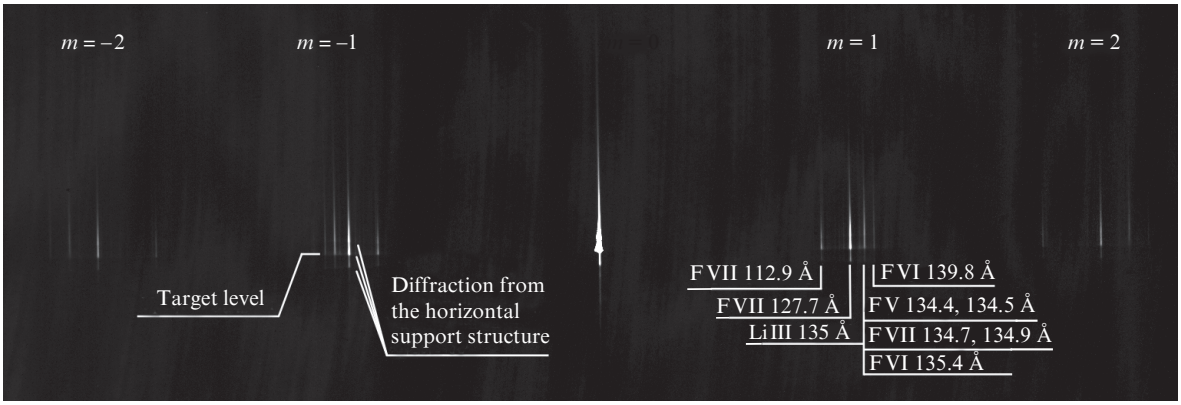

Figure 9. Stigmatic spectrum of the LiF plasma recorded in one laser shot of a Nd : YAG laser. Horizontally: the direction of dispersion. Vertically: the coordinate aligned with the entrance slit. One can see four bright line arrays of Li III, F V, F VI, and F VII ions in the first and second diffraction orders m. Observed vertically is the diffraction pattern due to the support structure: the sharp light-shadow boundary (corresponds to the level of the target surface) is seen three times in each line (the zeroth and two first diffraction orders).

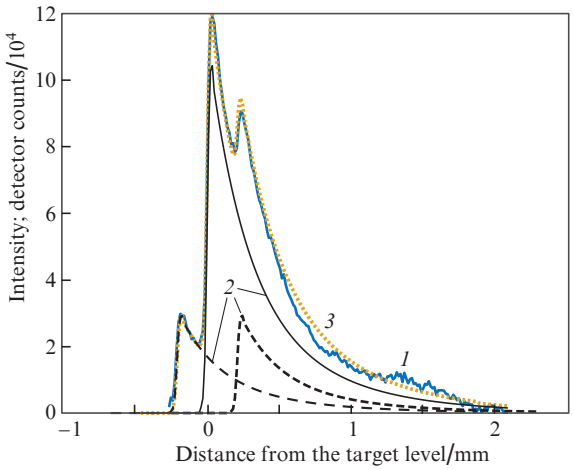

Figure 10. Experimentally recorded and reconstructed spatial intensity profiles of the $\lambda = 127.7$ Å F VII ion line; (*1*) detector readings (the sum of readings over several cells along the spectral line width); (*2*) reconstructed profile in the zeroth diffraction order (peaking at the level of the target surface) and two first orders (with their peaks at a level of 0.3 in intensity of the zeroth order maximum located at ±0.21 mm from the target level) of diffraction from the horizontal support structure; (*3*) total intensity of all three diffraction orders calculated from the reconstructed profile agrees nicely with the initial intensity distribution in the detector plane.

5. Conclusions

Normal-incidence mirrors based on aperiodic Mo/Be structures permit imaging in the wavelength range above 111 Å, making it possible to record space-resolved spectra. The attainable range width may be as large as an octave; in this case, the mirrors possess a uniform reflection coefficient at a level of 10%. These mirrors make it possible to extend the operating range of a broadband high-resolution imaging spectrometer [19, 20] towards shorter wavelengths.

The introduction of the layer thickness smoothing into the merit function employed in the design of aperiodic multilayer structures makes smoother the dependence of the layer thickness on the layer number in the structure. This is achieved at the expense of a small reflectivity lowering and an insignificant impairment in uniformity of the spectral reflection coefficient. The result of synthesis of these structures becomes more predictable: In this case, the effect of layer density–thickness relationship becomes smaller as does the error in deposited layer thickness. The smoothing yields good results for a relatively narrow range (111–138 Å), but its efficiency becomes lower with increasing range width. For this reason the structures with a uniform reflectivity in a broad (about an octave) range remain difficult to synthesise as before.

The Mo/Be mirrors based on a six-stack structure, which were synthesised at the IPM RAS, were employed to record space-resolved spectra in the 111–138 Å wavelength range using the configuration of an imaging diffraction spectrograph with a transmission grating. We obtained the line spectra from the laser-produced plasma of LiF and Mg targets and reconstructed the spatial intensity profile of the 127.7-Å line of F VI ions. The spectral resolving power of the instrument was about 160 (two CCD array detector pixels) and the spatial resolution turned out to be at a level of 50 μm (four CCD array pixels). The use of broadband Mo/Be mirrors in the configuration of a stigmatic spectrometer comprising a normal-incidence spherical mirror and a plane grazing-incidence varied line-space (VLS) reflection grating will make it possible to achieve a spectral resolving power of about 1000 and a spatial resolution at a level of two detector pixels (26 μm) in the range limited by the K edge of beryllium ($\lambda >$ 111 Å), much like was demonstrated with the use of a broadband Mo/Si mirror in the range limited by the L edge of silicon ($\lambda > 125$ Å) [19, 20].

Acknowledgements. The authors express their appreciation to A.S. Pirozhkov for his assistance in the modification of the multilayer structure optimisation code; to M.M. Barysheva, S.A. Garakhin, V.N. Polkovnikov, R.M. Smertin, and M.V. Svechnikov for the design, synthesis, and measurement of the Mo/Be mirror; as well as to F. Bijkerk for placing the transmission grating at our disposal.

References

1. Ragozin E.N., Andreev S.S., Bijkerk F., Kolachevsky N.N., Louis E., Pirozhkov A.S., Salashchenko N.N. *Proc. SPIE*, **3156**, 331 (1997).
2. Kolachevsky N.N., Pirozhkov A.S., Ragozin E.N. *Quantum Electron.*, **28**, 843 (1998) [*Kvantovaya Elektron.*, **25** (9), 867 (1998)].
3. Kirkpatrick P., Baez A.V. *J. Opt. Soc. Am.*, **38**, 766 (1948).

4. Weisskopf M.C., O'Dell S.L. *Proc. SPIE*, **3113**, 2 (1997).
5. Meekins J.F., Cruddace R.G., Gursky H. *Appl. Opt*., **26** (6), 990 (1987).
6. Van Loevezijn P., Schlatmann R., Verhoeven J., van Tiggelen B.A., Gullikson E.M. *Appl. Opt*., **35** (19), 3614 (1996).
7. Wang Z., Michette A.G. *J. Opt. A*: *Pure Appl. Opt*., **2**, 452 (2000).
8. Kolachevsky N.N., Pirozhkov A.S., Ragozin E.N. *Kratk. Soobshch. Fiz. FIAN*, (12), 55 (1998).
9. Kolachevsky N.N., Pirozhkov A.S., Ragozin E.N. *Quantum Electron*., **30** (5), 428 (2000) [*Kvantovaya Elektron*., **30** (5), 428 (2000)].
10. Kondratenko V.V., Levashov V.E., Pershin Yu.P., Pirozhkov A.S., Ragozin E.N. *Kratk. Soobshch. Fiz. FIAN*, (7), 32 (2001).
11. Zubarev E.N., Kondratenko V.V., Pol'tseva O.V., Sevryukova V.A., Fedorenko A.I., Yulin S.A. *Metallofizika i Noveishie Tekhnologii*, **19** (8), 56 (1997).
12. Pirozhkov A.S., Ragozin E.N. *Phys. Usp*., **58** (16), 1095 (2015) [*Usp. Fiz. Nauk*, **185** (11), 1203 (2015)].
13. Ragozin E.N., Levashov V.E., Mednikov K.N., Pirozhkov A.S., Sasorov P.V. *Proc. SPIE*, **4781**, 17 (2002).
14. Ragozin E.N., Kondratenko V.V., Levashov V.E., Pershin Yu.P., Pirozhkov A.S. *Proc. SPIE*, **4782**, 176 (2002).
15. Beigman I.L., Levashov V.E., Mednikov K.N., Pirozhkov A.S., Ragozin E.N., Tolstikhina I.Yu. *Quantum Electron*., **37** (11), 1060 (2007) [*Kvantovaya Elektron*., **37** (11), 1060 (2007)].
16. Beigman I.L., Vishnyakov E.A., Luginin M.S., Ragozin E.N., Tolstikhina I.Yu. *Quantum Electron*., **40** (6), 545 (2010) [*Kvantovaya Elektron*., **40** (6), 545 (2010)].
17. Kando M., Pirozhkov A.S., Kawase K., Esirkepov T.Zh., Fukuda Y., Kiriyama H., Okada H., Daito I., Kameshima T., Hayashi Y., Kotaki H., Mori M., Koga J.K., Daido H., Faenov A.Ya., Pikuz T., Ma J., Chen L.-M., Ragozin E.N., Kawach T., Kato Y., Tajima T., Bulanov S.V. *Phys. Rev. Lett*., **103** (23), 235003 (2009).
18. Pirozhkov A.S., Esirkepov T.Zh., Pikuz T.A., Faenov A.Ya., Ogura K., Hayashi Y., Kotaki H., Ragozin E.N., Neely D., Kiriyama H., Koga J.K., Fukuda Y., Sagisaka A., Nishikino M., Imazono T., Hasegawa N., Kawachi T., Bolton P.R., Daido H., Kato Y., Kondo K., Bulanov S.V., Kando M. *Sci. Rep*., **7**, 17968 (2017).
19. Shatokhin A.N., Kolesnikov A.O., Sasorov P.V., Vishnyakov E.A., Ragozin E.N. *Opt. Express*, **26** (15), 19009 (2018).
20. Vishnyakov E.A., Kolesnikov A.O., Kuzin A.A., Negrov D.V., Ragozin E.N., Sasorov P.V., Shatokhin A.N. *Quantum Electron*., **47** (1), 54 (2017) [*Kvantovaya Elektron*., **47** (1), 54 (2017)].
21. Ragozin E.N., Kondratenko V.V., Levashov V.E., Pershin Yu.P., Pirozhkov A.S. *Proc. SPIE*, **4782**, 176 (2002).
22. Svechnikov M., Pariev D., Nechay A., Salaschenko N., Chkhalo N., Vainer Y., Gaman D. *J. Appl. Crystallogr*., **50**, 1428 (2017).
23. Garakhin S.A., Zabrodin I.G., Zuev S.Yu., Kas'kov I.A., Lopatin A.Ya., Nechai A.N., Polkovnikov V.N., Salashchenko N.N., Tsybin N.N., Chkhalo N.I., Svechnikov M.V. *Quantum Electron*., **47** (4), 385 (2017) [*Kvantovaya Elektron*., **47** (4), 385 (2017)].
24. Svechnkov M.V., Chkhalo N.I., Gusev S.A., Nechay A.N., Pariev D.E., Pestov A.E., Polkovnikov V.N., Tatarsky D.A., Salaschenko N.N., Schäfers F., Sertsu M.G., Sokolov A., Vainer Y.A., Zorina M.V. *Opt. Express*, **26** (26), 33718 (2018).
25. Nechay A.N., Chkhalo N.I., Drozdov M.N., Garakhin S.A., Pariev D.E., Polkovnikov V.N., Salaschenko N.N., Svechnikov M.V., Vainer Yu.A., Meltchakov E., Delmotte F. *AIP Adv*., **8**, 075202 (2018).
26. Garakhin S.A., Mel'chakov E.N., Polkovnikov V.N., Salashchenko N.N., Chkhalo N.I. *Quantum Electron*., **47** (4), 378 (2017) [*Kvantovaya Elektron*., **47** (4), 378 (2017)].
27. Kozhevnikov I.V., Yakshin A.E., Bijkerk F. *Opt. Express*, **23** (7), 9276 (2015).
28. Kuhlman T., Yulin S.A., Feigl T., Kaiser N. *Proc. SPIE*, **4782**, 196 (2002).
29. Barysheva M.M., Garakhin S.A., Zuev S.Yu., Polkovnikov V.N., Salashchenko N.N., Svechnikov M.V., Smertin R.M., Chkhalo N.I., Meltchakov E. *Tech. Phys*., **64**, 1673 (2019) [*Zh. Tekh. Fiz*., **89** (11), 1763 (2019)].
30. Soufli R., Gullikson E.M. *Appl. Opt*., **37**, 1713 (1998).
31. Soufli R., Bajt S.E., Gullikson M. *Proc. SPIE*, **3767**, 251 (1999).
32. http://henke.lbl.gov/optical_constants/.